International Journal of
Drug Discovery and Pharmacology (IJDDP)

Scilight

Article

Check for updates

Inhibition of Trimethylamine Production by Targeting Bacterial BbuA-mediated γ-butyrobetaine Metabolism

Diana Zaca [1], Raitis Bobrovs [1], Kirill Shubin [1], Eduards Sevostjanovs [1], Dace Zigure [1], Aigars Jirgensons [1], Kaspars Tars [2,3], and Gints Kalnins [3,*]

[1] National Institute of Research and Innovation, Aizkraukles 21, LV-1006 Riga, Latvia
[2] Faculty of Medicine and Life Sciences, University of Latvia, Jelgavas 1, LV-1004, Riga, Latvia
[3] National Institute of Research and Innovation, Ratsupites 1 k-1, LV-1067 Riga, Latvia
* Correspondence: gints.kalnins@niri.lv
Received: 8 June 2026; Revised: 10 September 2026; Accepted: 12 October 2026; Published: 4 November 2026

Abstract: Trimethylamine (TMA) and its metabolite, trimethylamine-N oxide (TMAO), are chemical compounds of bacterial origin. TMA is produced in the human body by gut microbiota and further metabolized into TMAO by hepatic monooxygenase. High TMAO levels have been associated with several pathological conditions, including trimethylaminuria, atherosclerosis, renal failure, type 2 diabetes, and cancer. Preventing their production has been suggested to have a beneficial influence on health. In this study, we designed and tested substrate analogues of a recently discovered and characterized enzyme BbuA (γ-butyrobetaine-CoA oxidoreductase) and demonstrated that it is possible to suppress the TMA producing activity of BbuA enzyme with such designed inhibitors. Among the 12 compounds tested, two exhibited measurable but weak inhibitory activity, with IC_{50} values of 55.48 and 46.25 mM, respectively.

Keywords: trimethylamine; γ-butyrobetaine; BbuA

1. Introduction

The microbiome is widely recognized as a key determinant of human health, exerting diverse influences with implications that range from beneficial to harmful. Despite ongoing research, our understanding of these implications remains incomplete. Bacterial metabolites have been identified as potential agents influencing human health, and among them, trimethylamine (TMA) and its metabolite, trimethylamine-N oxide (TMAO), stand out as noteworthy examples. TMA is a simple organic compound, a tri-methylated derivative of ammonia. It is a volatile molecule, soluble in both water and fat, enabling it to easily traverse biological membranes. Mammalian organisms are incapable of synthesizing TMA, and thus, all TMA found in mammalian organisms originates either from diet or is produced by gut microbiota, which are able to produce TMA from compounds such as choline and L-carnitine [1,2].

In the human body, TMA can be further metabolized by hepatic flavin-containing monooxygenase 3 (FMO3) into TMAO [3]. However, disruptions in this metabolic process due to genetic mutations in the FMO3 gene can upset this balance [4,5]. Insufficient activity of FMO3 leads to the accumulation of TMA in the organism, and since TMA can easily permeate the skin, the excess is excreted through it. This genetic condition is known as trimethylaminuria or fish odor syndrome, characterized by the unpleasant odor resembling decaying fish. Elevated levels of TMAO have been associated with various pathological conditions, including cardiovascular diseases and atherosclerosis [1,6], renal failure [7], diabetes [8], and colorectal cancer [9]. The causative influence of TMAO on the development and progression of atherosclerosis in various model systems has been demonstrated in more than 20 studies over the past decade [6]. Consequently, blocking the production of TMA by gut microbiota has been proposed as an attractive target for preventing atherosclerosis [9,10].

TMA production is carried out by several bacterial enzyme systems. The most studied and currently considered the most relevant enzyme is CutC choline lyase, capable of producing TMA from choline [11,12]. It exhibits high specificity for choline, operates strictly under anaerobic conditions, and its abundance in the gut microbiota has been linked to elevated TMAO levels [13]. Its inhibition has been described in at least seven studies, with beneficial effects demonstrated in animal models in two cases [14–20]. CntA L-carnitine oxygenase has been shown to be capable of producing TMA from nutrients such as L-carnitine and γ-butyrobetaine [21,22]. However,

Copyright: © 2026 by the authors. This is an open access article under the terms and conditions of the Creative Commons Attribution (CC BY) license (https://creativecommons.org/licenses/by/4.0/).
Publisher's Note: Scilight stays neutral with regard to jurisdictional claims in published maps and institutional affiliations.

its relevance in the context of TMA production by gut microbiota has recently been questioned, as it requires oxygen for its catalysis, and its abundance in the gut microbiota has been found to have no correlation with TMAO levels in the organism [23]. CntA is thought to be a marginal contributor due to its oxygen requirement. Ergothionase cleaves ergothioneine, a thiourea derivative of histidine, into TMA and thiolurocanic acid. Several factors suggest that ergothionase could be relevant in the context of TMA production in the gastrointestinal system—the catalysis does not require oxygen, the enzyme is present in a few representatives of the gut microbiota, and it relies on the substrate ergothioneine, found in several types of food such as mushrooms and beans [24,25]. However, its influence on the TMA and TMAO pool in the mammalian organism has not been adequately evaluated thus far and remains unknown. TMAO reductase, or TorA, is a molybdenum-containing metalloenzyme that is part of the bacterial TMAO respiratory (Tor) system, using TMAO as a terminal acceptor in the electron transport chain [26]. As this enzyme performs a counter-reaction to FMO3, inhibiting it would have no relevance for the overall combined levels of TMA and TMAO in the human organism.

Recently, another anaerobic TMA producing pathway has been discovered by connecting *cai* and *bbu* operons. The *cai* operon, capable of the reversible conversion of L-carnitine into γ-butyrobetaine, has been known for decades [27–29]. It can utilize carnitine and crotobetaine as electron acceptors or, conversely, γ-butyrobetaine as an electron donor, depending on the environmental redox conditions. More recently, it was observed that after the rapid conversion of L-carnitine into γ-butyrobetaine, a low-abundance gut microbiota species in anaerobic conditions further converts it into TMA [30]. Even more recently, this last specific TMA conversion step was identified to be performed by *bbu* (or *gbu*) [31,32] and the abundance of this operon is predictive of TMA production in mouse gut microflora [33]. Consequently, the current understanding of L-carnitine metabolism by gut microbiota has been updated. The anaerobic metabolism of L-carnitine into TMA is now proposed to occur in two stages: the *cai* operon in one host converts L-carnitine into γ-butyrobetaine, and the *bbu* operon in another host converts γ-butyrobetaine into TMA and crotonyl-CoA. Even more, the abundance of faecal gbuA correlates with plasma TMAO, indicating its importance [32].

To date, no known host has been described as harboring both of *cai* and *bbu* loci, suggesting that this process likely occurs in polymicrobial environments [31]. Given that L-carnitine is the second most abundant dietary source of TMA after choline in the human diet, blocking its utilization could potentially play a crucial role in preventing TMA production in polymicrobial anaerobic conditions, such as those found in the gut microbiota.

In this research, we design and screen novel BbuA protein substrate analogue inhibitors using *in vitro* assays, and identify two prospective compounds able to block the production of TMA.

2. Materials and Methods

2.1. Synthesis of Substrate and Substrate Analogs

The synthesis of the substrate and all compounds tested is described in SI: Schemes S1–S10, Tables S1–S2 and Figures S1–S39; and also published in previous research [34–36].

2.2. Molecular Modeling Procedures

The potential BbuA inhibitors were docked in a docking model created by merging the AlphaFold model of *Emergencia timonensis* BbuA and the X-ray structure of the medium-chain acyl-CoA dehydrogenase in complex with transition state analog (PDB ID: 1UDY). The complex that consisted of BbuA AlphaFold model, 3-thiaoctanoyl-CoA, and FAD was prepared using Maestro Protein Preparation Wizard (Protein Preparation Workflow, Schrödinger Release 2024-4), minimized using Prime (Prime, Schrödinger Release 2024-4), and side chain protonation states were adjusted to pH 7.0. The docking grid was centered around the reference CoA analogue. The designed compounds were prepared for docking using LigPrep (LigPrep, Schrödinger Release 2024-4) by desalting the molecules, generating possible tautomers, and ionization states at pH 7.0 ± 2.0. Molecular docking was performed using Glide [37], with scaling of the van der Waals radii set to 0.9 for protein and ligand heavy atoms, and docking compounds flexibly. The top-scoring compounds were visually inspected for their ability to form hydrogen bonds similar to those established by the reference CoA analogue, with molecules showing internal strains or unsatisfied hydrogen bond donors being deprioritized. Docked poses were visualized using PyMOL (The PyMOL Molecular Graphics System, Version 3.0 Schrödinger, LLC).

2.3. In Vitro Enzymatic BbuA Assays

General procedures were adapted from previous work [31]. Unless specified contrary, all reagents were purchased from Merck. The *Emergencia timonensis bbuA* gene, together with the accompanying groES and groEL

genes, was ordered from BioCat and cloned into the pRSF-Duet-1 vector, with each gene placed under the control of a separate T7 promoter and terminator. Protein expression was carried out in BL21 (DE3) cells grown in 2 × TY medium supplemented with 0.2 mM riboflavin and 30 μg/mL kanamycin. Cultures were incubated at 37 °C with shaking at 200 rpm for approximately 2 h until an OD_{590} of 0.5–0.6 was reached. The cultures were then cooled to 15 °C for 30 min, followed by induction with 0.25 mM IPTG. After 24 h of expression, cells were harvested by centrifugation and immediately processed further for protein purification.

For lysis, 1 g of wet cell mass was resuspended in 5 mL of lysis buffer containing 50 mM potassium phosphate (pH 7.5), 300 mM NaCl, 10% (*v*/*v*) glycerol, 1 mM FAD, and 50 mM imidazole, and lysed by ultrasonication using a UP200S homogenizer (Hielscher). The lysate was clarified by centrifugation at 16,000× *g* for 30 min and incubated with Ni-NTA agarose (Merck) at a ratio of 1 mL resin per 10 mL lysate. The mixture was incubated on a rotator for 1 h at 7 °C, loaded onto a gravity-flow column, washed with lysis buffer followed by wash buffer (50 mM potassium phosphate, pH 7.5, 300 mM NaCl, 10% glycerol, and 100 mM imidazole), and finally eluted with elution buffer (wash buffer containing 300 mM imidazole). Eluted protein fractions were aliquoted, flash-frozen, and stored at −70 °C.

For enzymatic activity assays, the purified protein was concentrated to 200 μM and the buffer exchanged to 0.1 M Tris-HCl (pH 8.0) by using a 10 kDa ultrafiltration device (Millipore). 50 μL large reaction mixtures were assembled in 0.5 mL tubes in the following order: protein solution, 1 mM FAD, substrate analogs (final concentrations ranging from 50 to 0.02 mM), and the reaction was initiated by the addition of 1 mM GBB-CoA (Compound 1). After 5 min, reactions were terminated and trimethylamine (TMA) was stabilized in salt form by the addition of 5% formic acid. Samples were stored at −20 °C until analysis.

TMA concentrations were quantified by UPLC–MS/MS. Reported IC_{50} values represent the mean of three independent replicate experiments (Supplementary Dataset 1). In all cases, the positive control, defined as the BbuA reaction performed in the absence of added ligand, yielded TMA concentrations of no more than 200 μM, corresponding to less than 20% consumption of the initial substrate under the assay conditions.

The "N.D., >100 mM" designation was assigned to compounds for which we could not reliably detect more than a 10% reduction in activity relative to the positive control at ligand concentrations of 40–50 mM, corresponding to estimated IC_{50} values far above 100 mM. We did not test concentrations above 50 mM because of solubility limitations and the potential for nonspecific inhibition at higher ligand concentrations.

2.4. UPLC-MS/MS TMA Quantification Analysis

A Waters Xevo TQ-S Micro tandem mass spectrometer in positive ionization electrospray mode with a Waters Acquity UPLC H-class system was used to perform the analysis. Chromatographic separation was achieved on an Acquity UPLC BEH HILIC column (2.1 × 50 mm, 1.7 μm) in gradient mode with 10 mM ammonium acetate buffer (pH 4.0) as mobile phase A and acetonitrile as mobile phase B. The flow rate was 0.4 mL/min with a column temperature of 50 °C. The gradient program was: 0 min at 10% A, 3.5 min at 10% A, 4.5 min at 60% A, 8 min at 60% A, 8.2 min at 10% A, and 10 min at 10% A. Capillary voltage was 3.0 kV, source temperature was 140 °C, desolvation gas temperature was 600 °C at a flow rate of 800 L/h, cone voltage was 30 V, and collision energy was 15 eV. Quantification was performed by integration of the multiple-reaction monitoring trace of TMA (60.1 >> 45.0 Da). The calibration range was from 0.5 μM to 300 μM. The samples were diluted fivefold with acetonitrile/methanol mixture (3:1, *v*/*v*).

3. Results

3.1. Rational Design of BbuA Inhibitor Candidates

Our inhibitor design strategy was based on blocking the BbuA-catalyzed α,β-dehydrogenation reaction by replacing the α and/or β C–H bonds with non-reactive substituents resistant to enzymatic hydrogen abstraction, thereby preventing formation of the corresponding unsaturated intermediate. The proposed catalytic mechanism of BbuA-catalyzed α,β-dehydrogenation [38] and the inhibitor design strategy are illustrated in Figure 1.

To evaluate this hypothesis, we prepared a focused panel of trimethylammonium-containing acyl derivatives including coenzyme A (CoA) thioesters (compounds **3, 5, 6, 7, 8, 10, 11, 12** and **13**, SI) and truncated CoA surrogates, including SNAC (N-acetylcysteamine; compound **2**, SI) and PAN (pantetheine; compounds **4** and **9**, SI) derivatives. The series systematically varied steric properties, conformational flexibility, and π-character of the acyl backbone by incorporating linear, α-branched, α,β-unsaturated, aryl, and conformationally constrained cyclic scaffolds, while preserving the permanently charged N,N,N-trimethylammonium group characteristic of the native substrate.

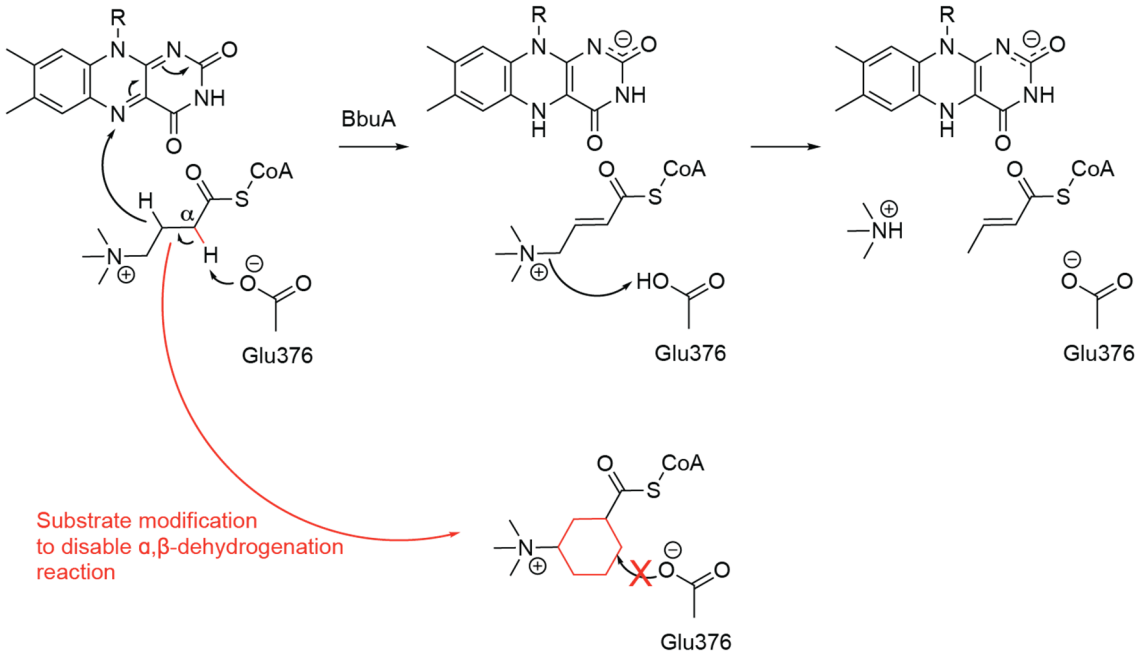


Figure 1. The proposed chemical mechanism of BbuA-catalyzed α,β-dehydrogenation and the inhibition strategy.

3.2. Synthesis of CoA Thioesters and Surrogate Analogues

The principal synthetic challenge was the high polarity and zwitterionic nature of the target acids and thioesters, which complicated activation, solubility, and purification. To overcome these limitations, we adopted a convergent synthetic route in which all analogues were first converted into the corresponding quaternary ammonium carboxylic acids, followed by a common thioesterification sequence. Depending on the scaffold, the quaternary ammonium acids were prepared either by quaternization of ω-halo esters with trimethylamine or by exhaustive methylation of amine precursors for conformationally constrained cyclic analogues.

Several approaches to CoA acylation have been reported; however, many protocols are substrate-specific and are not readily transferable across highly polar betaines [39–41]. Since CoA acylation is typically performed in aqueous base (pH 8–9), the use of activated trimethylammonium-substituted carboxylic acids is limited by rapid hydrolysis. In our hands, commonly used activation methods—PyBOP ((Benzotriazol-1-yloxy)tripyrrolidinophosphonium hexafluorophosphate) [42], ethyl chloroformate [43], carbonyldiimidazole [44,45], HBTU((benzotriazol-1-yl)-N,N,N′,N′-tetramethyluronium hexafluorophosphate) [46], and COMU (1-[(1-(Cyano-2-ethoxy-2-oxoethylideneaminooxy)dimethylaminomorpholino)]uronium hexafluorophosphate) [47]—were inefficient when applied to betaines or betaine salts.

We therefore employed direct CoA thioesterification using in situ-generated symmetric anhydrides [41,48]. To facilitate anhydride formation, chloride counterions were exchanged for the more lipophilic hexafluorophosphate (PF_6^-), which substantially improved substrate solubility in acetonitrile. The resulting PF_6^- salts were converted into symmetric anhydrides by N,N′-dicyclohexylcarbodiimide (DCC)-mediated dehydration in an aprotic solvent.

The activated anhydrides were used without isolation and added dropwise as acetonitrile solutions to CoA in 0.5 M aqueous $NaHCO_3$. Reactions were typically complete within 30 min at room temperature and were quenched by acidification to approximately pH 3. Smaller thioester surrogates were prepared in parallel: the SNAC thioester (compound **2**) was synthesized by HBTU-mediated coupling, whereas PAN thioesters DI-1462 (SI) and **9** were obtained using the same anhydride intermediates employed for CoA coupling. All products were purified by reverse-phase C18 chromatography. Overall, the PF_6^-/symmetric anhydride strategy provided a practical and unified route to a structurally diverse library of betaine-derived CoA thioesters and truncated surrogates and should be readily extensible to additional analogues.

3.3. In Vitro Inhibition of BbuA

The potency of all synthesized CoA thioesters and substrate analogues was tested in a UPLC–MS/MS-based *in vitro* assay, using purified BbuA enzyme from *Emergencia timonensis* as a target. Of all synthesized

compounds, only GBB-CoA derivatives containing the cyclopropane (**5**) and cyclohexane (**8**) moieties displayed measurable inhibitory potency, with IC_{50} values of 46.25 and 55.48 mM, respectively (Table 1, Supplementary Dataset 1). Nonspecific inhibition at ligand concentrations of approximately 40–50 mM cannot be completely excluded. However, several observations argue against these effects being the primary cause of the observed inhibition. In particular, structurally similar compounds 10–12 did not exhibit comparable inhibitory activity under the same experimental conditions, despite being structurally very similar.

Molecular modeling suggests that these cyclized analogues mimic the binding mode of the native substrate (Figure 2). In these compounds, the structural modifications do not alter the conformation of the γ-butyrobetaine core, preserving the ionic interaction between the trimethylammonium group and Asp89. To assess the role of the CoA moiety, analogue **9** was synthesized by combining the cyclohexane motif of compound **8** with pantetheine (PAN), a truncated CoA precursor. However, this truncation resulted in a complete loss of potency, indicating that key interactions mediated by the intact CoA group are essential for binding. Replacing the cyclohexane ring of **8** with an aromatic moiety (**6**) similarly abolished inhibitory activity. Molecular docking indicates that the restricted conformational flexibility of the benzyl-containing γ-butyrobetaine bioisostere prevents optimal positioning of the trimethylammonium group within the active site. Neither the dehydrogenated analogue (**7**) nor the methylated analogues (**3**, **4**) inhibited BbuA. For compound **7**, the lack of activity is likely due to conformational rigidity preventing the γ-butyrobetaine bioisostere from adopting its bioactive conformation. Similarly, the cyclopropane derivative lacking the trimethylamine moiety (**13**) was inactive, confirming the necessity of this functional group for target inhibition. Reliable inhibition data could not be determined for compounds **10–12**, and they were excluded from further evaluation.

Table 1. Tested compounds and BbuA *in vitro* enzymatic assay results.

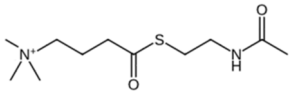
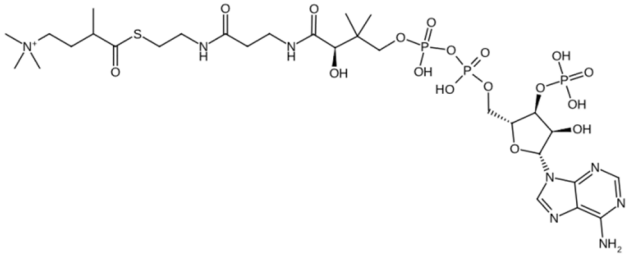
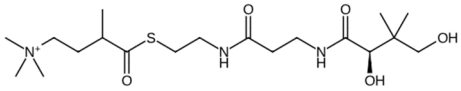
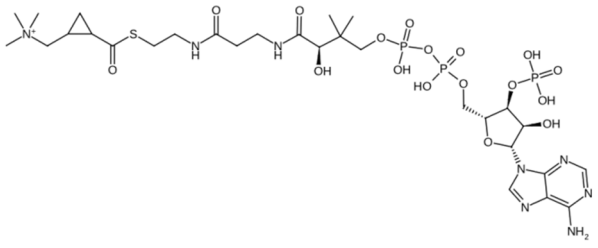
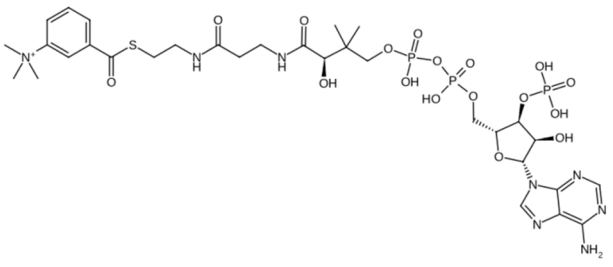
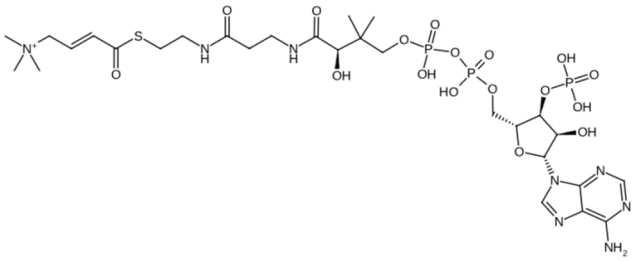
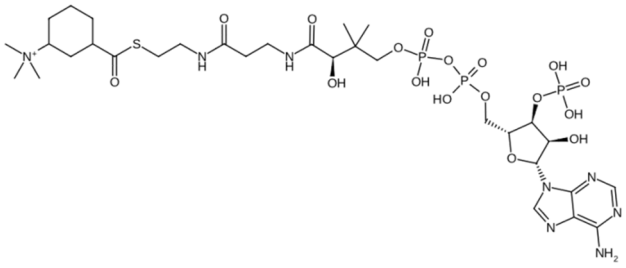
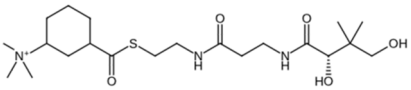
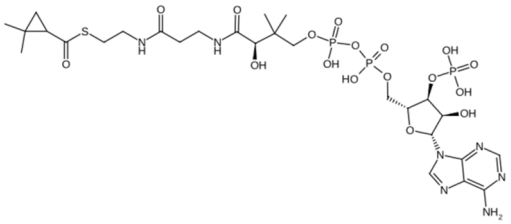
Compound Designation	Compound	IC_{50} BbuA *In Vitro* Test Result
Compound **2**		N.D., >100 mM
Compound **3**		N.D., >100 mM
Compound **4**		N.D., >100 mM
Compound **5**		46.25 ± 6.5 mM
Compound **6**		N.D., >100 mM

Table 1. *Cont.*

Compound Designation	Compound	IC_{50} BbuA *In Vitro* Test Result
Compound **7**		N.D., >100 mM
Compound **8**		55.48± 5.5 mM
Compound **9**		N.D., >100 mM
Compound **13**		N.D., >100 mM

N.D.—not detected.

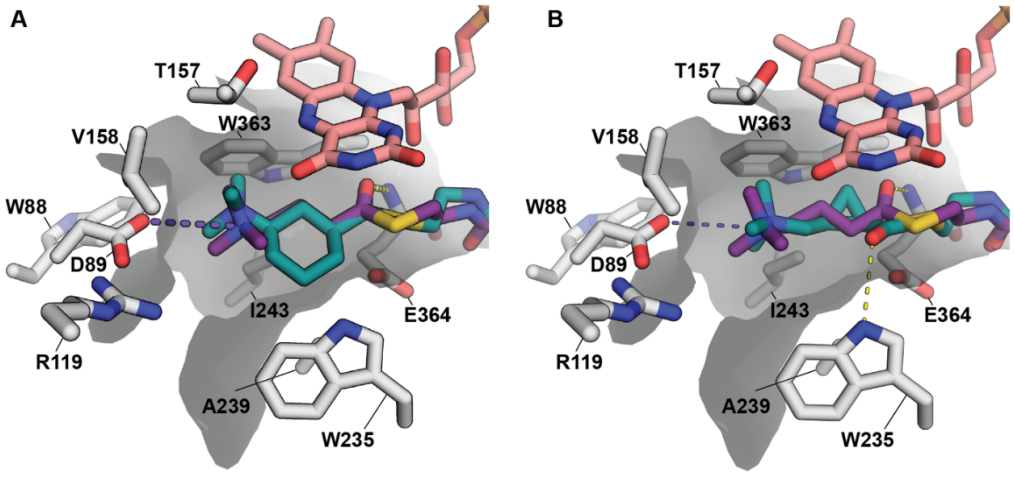


Figure 2. The modelled pose of compounds (**A**) **8** and (**B**) **5** (teal) and γ-butyrobetainyl-CoA (compound **1**, purple) in the active site of the *Emergencia timonensis* BbuA. Ligand, substrate, FAD (salmon), and binding site residue side chains are shown as sticks. Hydrogen atoms are omitted for clarity. Hydrogen and ionic bonds are shown as yellow and purple dashed lines, respectively.

4. Discussion

The inhibitor design was based on a mechanism-guided strategy aimed at preventing the initial α,β-dehydrogenation step catalyzed by BbuA through replacement of abstractable α- and β-hydrogen atoms with

metabolically inert substituents. Although the resulting inhibitors displayed only modest potency, the observed inhibition of compounds **5** and **8** demonstrates that this approach can interfere with BbuA catalysis. When compared with other reported inhibitors of microbial TMA production, the compounds identified in the present study exhibit relatively low potency. For example, fluoromethylcholine (FMC) has been reported to inhibit CutC in the nanomolar range [15], whereas the most potent reported CntA inhibitors exhibit low-micromolar activity [22]. In contrast, the GBB-CoA analogs identified here display substantially weaker inhibitory activity. Their structural complexity and highly hydrophilic character may, however, limit passive diffusion across bacterial cell membranes, potentially resulting in low intracellular exposure and reduced effective concentrations at the target enzyme. An additional consideration is their potential selectivity toward microbial metabolic pathways. Because no known human enzyme directly utilizes GBB-CoA as a substrate, GBB-CoA analogs may have a reduced propensity for off-target interactions with human metabolic enzymes and for the generation of unintended human metabolites. This could represent a potential safety advantage over compounds such as FMC, for which interactions with mammalian choline-metabolizing pathways, including choline kinase and choline acetyltransferase, may warrant further investigation.

The inactivity of the truncated analogues and derivatives lacking either the trimethylammonium or ADP moiety suggests that productive binding requires recognition of multiple regions of the native substrate. In particular, the absence of activity for compounds **9** and **13** indicates that both the trimethylammonium headgroup and the CoA-derived ADP portion contribute substantially to enzyme binding, as this type of truncation abolishes activity. Likewise, the lack of inhibition by the SNAC and pantetheine analogues indicates that the phosphoadenosine portion of CoA cannot be readily replaced by shorter thioester surrogates without substantial loss of affinity.

Among the full-length CoA analogues, only compounds incorporating conformationally constrained cyclic scaffolds produced detectable inhibition, whereas linear, α-branched, α,β-unsaturated, and aromatic analogues were inactive. These findings suggest that conformational restriction of the acyl chain may improve positioning within the active site and partially compensate for the loss of catalytic turnover, although the high IC_{50} values indicate that substantial optimization will be required to achieve pharmacologically relevant potency. Given the tightly enclosed nature of the BbuA active-site pocket and its limited capacity to accommodate additional structural modifications, further optimization of inhibitors based directly on the CoA–γ-butyrobetaine substrate scaffold may offer limited potential for improving potency. Therefore, alternative strategies for suppressing anaerobic TMA production from γ-butyrobetaine should also be considered. One such approach would be to target the initial step catalyzed by the BbuBC CoA acyltransferase, as previously proposed [31,32].

Overall, this study provides the first examples of enzymatic inhibition of BbuA and suppression of TMA production using targeted inhibitor ligands. Our results suggest that both the trimethylammonium and ADP moieties represent critical pharmacophores for effective ligand binding within the BbuA active site. Furthermore, incorporation of conformationally constrained cyclic scaffolds into trimethylammonium-containing CoA thioesters may provide a useful strategy for improving inhibitory activity in future generations of BbuA inhibitors.

5. Conclusions

We developed a library of trimethylammonium-containing CoA thioesters and established a PF_6^-/symmetric anhydride form use for their synthesis. Cyclopropane and cyclohexane CoA derivatives were identified as the first BbuA inhibitors, demonstrating proof of concept for targeted suppression of TMA production. Activity depended on the presence of both the trimethylammonium and ADP moieties, while cyclic acyl scaffolds improved inhibitory effects.

Supplementary Materials: The following supporting information can be downloaded at: https://media.sciltp.com/articles/others/2611031601178856/IJDDP-2026-000012_Supplementary_Materials.zip. Scheme S1: Synthesis of compounds **1** (DI-1382) and 2 (DI-1502); Scheme S2: Synthesis of compounds **3** (DI-1455) and 4 (DI-1462); Scheme S3: Synthesis of compound 5 (DI-1483); Scheme S4: Synthesis of compound **6** (DI-1573); Scheme S5: Synthesis of compound **7** (DI-1580); Scheme S6: Synthesis of compounds **8** (DI-1593) and **9** (DI-1464); Scheme S7: Synthesis of compound **10** (DI-1639); Scheme S8: Synthesis of compound **11** (DI-1664); Scheme S9: Synthesis of compound **12** (DI-1678); Scheme S10: Synthesis of compound **13** (DI-1271); Table S1: Correspondence between manuscript compound numbers, internal DI codes, synthetic schemes, and analytical figures; Table S2: NMR assignments abbreviations; Figure S1: ^{1}H NMR (400 MHz, D_2O) spectrum of compound **1** (DI-1382); Figure S2: ^{13}C NMR (101 MHz, D_2O) spectrum of compound **1** (DI-1382); Figure S3: HRMS (ESI^+, TOF) spectrum of compound **1** (DI-1382); Figure S4: ^{1}H NMR (400 MHz, D_2O) spectrum of compound **2** (DI-1502); Figure S5: ^{13}C NMR (101 MHz, D_2O) spectrum of compound **2** (DI-1502); Figure S6: HRMS (ESI^+, TOF) spectrum of compound **2** (DI-1502); Figure S7: ^{1}H NMR (400 MHz, D_2O) spectrum of compound **3** (DI-1455); Figure S8: ^{13}C NMR (101 MHz, D_2O) spectrum of compound **3** (DI-1455); Figure S9: HRMS (ESI^+, TOF) spectrum of compound **3** (DI-1455); Figure S10: ^{1}H NMR (400 MHz, D_2O) spectrum of compound **4** (DI-1462); Figure S11: ^{13}C NMR (101 MHz, D_2O) spectrum of compound **4** (DI-1462); Figure S12: HRMS (ESI^+, TOF) spectrum of compound **4** (DI-1462); Figure S13: ^{1}H NMR (400 MHz, D_2O) spectrum of compound **5** (DI-1483); Figure S14: ^{13}C NMR (101 MHz, D_2O) spectrum of compound **5** (DI-1483); Figure S15: HRMS (ESI^+, TOF) spectrum of compound **5** (DI-1483); Figure S16: ^{1}H NMR (400 MHz, D_2O) spectrum of compound **6** (DI-1573); Figure S17:

^{13}C NMR (101 MHz, D_2O) spectrum of compound **6** (DI-1573); Figure S18: HRMS (ESI^+, TOF) spectrum of compound **6** (DI-1573); Figure S19: ^{1}H NMR (400 MHz, D_2O) spectrum of compound **7** (DI-1580); Figure S20: ^{13}C NMR (101 MHz, D_2O) spectrum of compound **7** (DI-1580); Figure S21: HRMS (ESI^+, TOF) spectrum of compound **7** (DI-1580); Figure S22: ^{1}H NMR (400 MHz, D_2O) spectrum of compound **8** (DI-1593); Figure S23: ^{13}C NMR (101 MHz, D_2O) spectrum of compound **8** (DI-1593); Figure S24: HRMS (ESI^+, TOF) spectrum of compound **8** (DI-1593); Figure S25: ^{1}H NMR (400 MHz, D_2O) spectrum of compound **9** (DI-1464); Figure S26: ^{13}C NMR (101 MHz, D_2O) spectrum of compound **9** (DI-1464); Figure S27: HRMS (ESI^+, TOF) spectrum of compound **9** (DI-1464); Figure S28: ^{1}H NMR (400 MHz, D_2O) spectrum of compound **10** (DI-1639); Figure S29: ^{13}C NMR (101 MHz, D_2O) spectrum of compound **10** (DI-1639); Figure S30: HRMS (ESI^+, TOF) spectrum of compound **10** (DI-1639); Figure S31: ^{1}H NMR (400 MHz, D_2O) spectrum of compound **11** (DI-1664); Figure S32: ^{13}C NMR (101 MHz, D_2O) spectrum of compound **11** (DI-1664); Figure S33: HRMS (ESI^+, TOF) spectrum of compound **11** (DI-1664); Figure S34: ^{1}H NMR (400 MHz, D_2O) spectrum of compound **12** (DI-1678); Figure S35: ^{13}C NMR (101 MHz, D_2O) spectrum of compound **12** (DI-1678); Figure S36: HRMS (ESI^+, TOF) spectrum of compound **12** (DI-1678); Figure S37: ^{1}H NMR (400 MHz, D_2O) spectrum of compound **13** (DI-1271); Figure S38: ^{13}C NMR (101 MHz, D_2O) spectrum of compound 13 (DI-1271); Figure S39: HRMS (ESI^+, TOF) spectrum of compound **13** (DI-1271).

Author Contributions: G.K., K.T. and R.B.—study design and conception; D.Z. (Diana Zaca), R.B., K.S., E.S., D.Z. (Dace Zigure), A.J. and G.K.—experimental investigation; G.K., K.S., R.B. and D.Z. (Diana Zaca)—manuscript writing and editing. All authors have read and agreed to the published version of the manuscript.

Funding: This research was supported within the framework of the European Union's Recovery and Resilience Mechanism project No.5.2.1.1.i.0/2/24/I/CFLA/001 "Consolidation of the Latvian Institute of Organic Synthesis and the Latvian Biomedical Research and Study Centre".

Institutional Review Board Statement: Not applicable.

Informed Consent Statement: Not applicable.

Data Availability Statement: The data that supports the findings of this study are available in Supporting Information of this article.

Conflicts of Interest: The authors declare no conflicts of interest.

Use of AI and AI-Assisted Technologies: During the preparation of this work, the authors used GPT-5.6, strictly for language polishing only. After using this tool, the authors reviewed and edited the content as needed and take full responsibility for the content of the published article.

Abbreviations: TMA—trimethylamine; TMAO—trimethylamine-N oxide; FMO3—flavin-containing monooxygenase 3; SNAC—N-acetylcysteamine; PAN—pantetheine; DCC—N,N′-dicyclohexylcarbodiimide; PyBOP—(Benzotriazol-1-yloxy) tripyrrolidinophosphonium hexafluorophosphate; HBTU—(benzotriazol-1-yl)-N,N,N′,N′-tetramethyluronium hexafluorophosphate; COMU—1-[(1-(Cyano-2-ethoxy-2-oxoethylideneaminooxy)dimethylaminomorpholino)]uronium hexafluorophosphate; FMC—fluoromethylcholine; FAD—flavin adenine dinucleotide, IPTG—isopropyl β-D-1-thiogalactopyranoside, GBB—γ-butyrobetaine, ADP—adenosine diphosphate, UPLC—ultra-performance liquid chromatography, MS/MS—tandem mass spectrometry, HILIC—hydrophilic interaction liquid chromatography, ESI—electrospray ionization.

References

1. Wang, Z.; Klipfell, E.; Bennett, B.J.; et al. Gut flora metabolism of phosphatidylcholine promotes cardiovascular disease. *Nature* **2011**, *472*, 57–63. https://doi.org/10.1038/nature09922.
2. Koeth, R.A.; Levison, B.S.; Culley, M.K.; et al. γ-Butyrobetaine Is a Proatherogenic Intermediate in Gut Microbial Metabolism of L-Carnitine to TMAO. *Cell Metab.* **2014**, *20*, 799–812. https://doi.org/10.1016/j.cmet.2014.10.006.
3. Lang, D.; Yeung, C.; Peter, R.; et al. Isoform specificity of trimethylamine N-oxygenation by human flavin-containing monooxygenase (FMO) and P450 enzymes: Selective catalysis by FMO3. *Biochem. Pharmacol.* **1998**, *56*, 1005–1012. https://doi.org/10.1016/s0006-2952(98)00218-4.
4. Dolphin, C.T.; Janmohamed, A.; Smith, R.L.; et al. Missense mutation in flavin-containing mono-oxygenase 3 gene, FMO3, underlies fish-odour syndrome. *Nat. Genet.* **1997**, *17*, 491–494. https://doi.org/10.1038/ng1297-491.
5. Treacy, E.P.; Akerman, B.R.; Chow, L.M.; et al. Mutations of the flavin-containing monooxygenase gene (FMO3) cause trimethylaminuria, a defect in detoxication. *Hum. Mol. Genet.* **1998**, *7*, 839–845. https://doi.org/10.1093/hmg/7.5.839.
6. Oktaviono, Y.H.; Dyah Lamara, A.; Saputra, P.B.T.; et al. The roles of trimethylamine-N-oxide in atherosclerosis and its potential therapeutic aspect: A literature review. *Biomol. Biomed.* **2023**, *23*, 936–948. https://doi.org/10.17305/bb.2023.8893.
7. Tang, W.H.W.; Wang, Z.; Kennedy, D.J.; et al. Gut Microbiota-Dependent Trimethylamine *N* -Oxide (TMAO) Pathway Contributes to Both Development of Renal Insufficiency and Mortality Risk in Chronic Kidney Disease. *Circ. Res.* **2015**, *116*, 448–455. https://doi.org/10.1161/circresaha.116.305360.
8. Dambrova, M.; Latkovskis, G.; Kuka, J.; et al. Diabetes is Associated with Higher Trimethylamine N-oxide Plasma Levels. *Exp. Clin. Endocrinol. Diabetes* **2016**, *124*, 251–256. https://doi.org/10.1055/s-0035-1569330.

9. Xu, R.; Wang, Q.; Li, L. A genome-wide systems analysis reveals strong link between colorectal cancer and trimethylamine N-oxide (TMAO), a gut microbial metabolite of dietary meat and fat. *BMC Genom.* **2015**, *16* (Suppl. S7), S4.
10. Jing, L.; Zhang, H.; Xiang, Q.; et al. Targeting Trimethylamine N-Oxide: A New Therapeutic Strategy for Alleviating Atherosclerosis. *Front. Cardiovasc. Med.* **2022**, *9*, 864600. https://doi.org/10.3389/fcvm.2022.864600.
11. Craciun, S.; Balskus, E.P. Microbial conversion of choline to trimethylamine requires a glycyl radical enzyme. *Proc. Natl. Acad. Sci. USA* **2012**, *109*, 21307–21312. https://doi.org/10.1073/pnas.1215689109.
12. Kalnins, G.; Kuka, J.; Grinberga, S.; et al. Structure and Function of CutC Choline Lyase from Human Microbiota Bacterium Klebsiella pneumoniae. *J. Biol. Chem.* **2015**, *290*, 21732–21740. https://doi.org/10.1074/jbc.m115.670471.
13. Dalla Via, A.; Gargari, G.; Taverniti, V.; et al. Urinary TMAO Levels Are Associated with the Taxonomic Composition of the Gut Microbiota and with the Choline TMA-Lyase Gene (cutC) Harbored by Enterobacteriaceae. *Nutrients* **2020**, *12*, 62. https://doi.org/10.3390/nu12010062.
14. Wang, Z.; Roberts, A.B.; Buffa, J.A.; et al. Non-lethal Inhibition of Gut Microbial Trimethylamine Production for the Treatment of Atherosclerosis. *Cell* **2015**, *163*, 1585–1595. https://doi.org/10.1016/j.cell.2015.11.055.
15. Roberts, A.B.; Gu, X.; Buffa, J.A.; et al. Development of a gut microbe–targeted nonlethal therapeutic to inhibit thrombosis potential. *Nat. Med.* **2018**, *24*, 1407–1417. https://doi.org/10.1038/s41591-018-0128-1.
16. Orman, M.; Bodea, S.; Funk, M.A.; et al. Structure-Guided Identification of a Small Molecule That Inhibits Anaerobic Choline Metabolism by Human Gut Bacteria. *J. Am. Chem. Soc.* **2019**, *141*, 33–37. https://doi.org/10.1021/jacs.8b04883.
17. Bollenbach, M.; Ortega, M.; Orman, M.; et al. Discovery of a Cyclic Choline Analog That Inhibits Anaerobic Choline Metabolism by Human Gut Bacteria. *ACS Med. Chem. Lett.* **2020**, *11*, 1980–1985. https://doi.org/10.1021/acsmedchemlett.0c00005.
18. Gabr, M.T.; Machalz, D.; Pach, S.; et al. A benzoxazole derivative as an inhibitor of anaerobic choline metabolism by human gut microbiota. *RSC Med. Chem.* **2020**, *11*, 1402–1412. https://doi.org/10.1039/d0md00218f.
19. Gabr, M.; Świderek, K. Discovery of a Histidine-Based Scaffold as an Inhibitor of Gut Microbial Choline Trimethylamine-Lyase. *ChemMedChem* **2020**, *15*, 2273–2279. https://doi.org/10.1002/cmdc.202000571.
20. Gabr, M.T.; Deganutti, G.; Reynolds, C.A. Peptidomimetic-based approach toward inhibitors of microbial trimethylamine lyases. *Chem. Biol. Drug Des.* **2021**, *97*, 231–236. https://doi.org/10.1111/cbdd.13775.
21. Zhu, Y.; Jameson, E.; Crosatti, M.; et al. Carnitine metabolism to trimethylamine by an unusual Rieske-type oxygenase from human microbiota. *Proc. Natl. Acad. Sci. USA* **2014**, *111*, 4268–4273. https://doi.org/10.1073/pnas.1316569111.
22. Quareshy, M.; Shanmugam, M.; Townsend, E.; et al. Structural basis of carnitine monooxygenase CntA substrate specificity, inhibition, and intersubunit electron transfer. *J. Biol. Chem.* **2021**, *296*, 100038. https://doi.org/10.1074/jbc.ra120.016019.
23. Wu, W.K.; Chen, C.C.; Liu, P.Y.; et al. Identification of TMAO-producer phenotype and host–diet–gut dysbiosis by carnitine challenge test in human and germ-free mice. *Gut* **2019**, *68*, 1439–1449. https://doi.org/10.1136/gutjnl-2018-317155.
24. Maurer, A.; Leisinger, F.; Lim, D.; et al. Structure and Mechanism of Ergothionase from *Treponema denticola*. *Chem. Eur. J.* **2019**, *25*, 10298–10303. https://doi.org/10.1002/chem.201901866.
25. Muramatsu, H.; Matsuo, H.; Okada, N.; et al. Characterization of ergothionase from Burkholderia sp. HME13 and its application to enzymatic quantification of ergothioneine. *Appl. Microbiol. Biotechnol.* **2013**, *97*, 5389–5400. https://doi.org/10.1007/s00253-012-4442-0.
26. Méjean, V.; Iobbi-Nivol, C.; Lepelletier, M.; et al. TMAO anaerobic respiration in Escherichia coli: Involvement of the tor operon. *Mol. Microbiol.* **1994**, *11*, 1169–1179. https://doi.org/10.1111/j.1365-2958.1994.tb00393.x.
27. Rebouche, C.J.; Seim, H. Carnitine Metabolism and Its Regulation in Microorganisms and Mammals. *Annu. Rev. Nutr.* **1998**, *18*, 39–61. https://doi.org/10.1146/annurev.nutr.18.1.39.
28. Engemann, C.; Elssner, T.; Pfeifer, S.; et al. Identification and functional characterisation of genes and corresponding enzymes involved in carnitine metabolism of *Proteus* sp. *Arch. Microbiol.* **2005**, *183*, 176–189. https://doi.org/10.1007/s00203-005-0760-2.
29. Elssner, T.; Engemann, C.; Baumgart, K.; et al. Involvement of Coenzyme A Esters and Two New Enzymes, an Enoyl-CoA Hydratase and a CoA-Transferase, in the Hydration of Crotonobetaine to L-Carnitine by *Escherichia coli*. *Biochemistry* **2001**, *40*, 11140–11148. https://doi.org/10.1021/bi0108812.
30. Koeth, R.A.; Lam-Galvez, B.R.; Kirsop, J.; et al. l-Carnitine in omnivorous diets induces an atherogenic gut microbial pathway in humans. *J. Clin. Investig.* **2019**, *129*, 373–387. https://doi.org/10.1172/jci94601.
31. Rajakovich, L.J.; Fu, B.; Bollenbach, M.; et al. Elucidation of an anaerobic pathway for metabolism of L-carnitine–derived γ-butyrobetaine to trimethylamine in human gut bacteria. *Proc. Natl. Acad. Sci. USA* **2021**, *118*, e2101498118. https://doi.org/10.1073/pnas.2101498118.
32. Buffa, J.A.; Romano, K.A.; Copeland, M.F.; et al. The microbial gbu gene cluster links cardiovascular disease risk associated with red meat consumption to microbiota l-carnitine catabolism. *Nat. Microbiol.* **2022**, *7*, 73–86. https://doi.org/10.1038/s41564-021-01010-x.

33. Wu, W.K.; Lo, Y.L.; Chiu, J.Y.; et al. Gut microbes with the gbu genes determine TMAO production from L-carnitine intake and serve as a biomarker for precision nutrition. *Gut Microbes* **2025**, *17*, 2446374. https://doi.org/10.1080/19490976.2024.2446374.
34. Cui, L.Q.; Dong, Z.L.; Liu, K.; et. al. Design, synthesis, structure, and dehydrogenation reactivity of a water-soluble o-iodoxybenzoic acid derivative bearing a trimethylammonium group. *Org. Lett.* **2011**, *13*, 6488–6491. https://doi.org/10.1021/ol202777h.
35. Badland, M.; Bains, C.A.; Howard, R.; et al. An improved synthesis of (1R,3S)-3-[(tert-butoxycarbonyl)amino] cyclohexanecarboxylic acid. *Tetrahedron: Asymmetry* **2010**, *21*, 864–866. https://doi.org/10.1016/j.tetasy.2010.04.049.
36. Tars, K.; Leitans, J.; Kazaks, A.; et al. Targeting carnitine biosynthesis: discovery of new inhibitors against γ-butyrobetaine hydroxylase. *J. Med. Chem.* **2014**, *57*, 2213–2236. https://doi.org/10.1021/jm401603e.
37. Friesner, R.A.; Banks, J.L.; Murphy, R.B.; et al. Glide: A New Approach for Rapid, Accurate Docking and Scoring. 1. Method and Assessment of Docking Accuracy. *J. Med. Chem.* **2004**, *47*, 1739–1749. https://doi.org/10.1021/jm0306430.
38. Ghisla, S.; Thorpe, C. Acyl-CoA dehydrogenases. A mechanistic overview. *Eur. J. Biochem.* **2004**, *271*, 494–508. https://doi.org/10.1046/j.1432-1033.2003.03946.x.
39. Elssner, T.; Hennig, L.; Frauendorf, H.; et al. Isolation, Identification, and Synthesis of γ-Butyrobetainyl-CoA and Crotonobetainyl-CoA, Compounds Involved in Carnitine Metabolism of *E. coli*. *Biochemistry* **2000**, *39*, 10761–10769. https://doi.org/10.1021/bi000776c.
40. Olsen, J.; Li, C.; Bjørnsdottir, I.; et al. *In Vitro* and *in Vivo* Studies on Acyl-Coenzyme A-Dependent Bioactivation of Zomepirac in Rats. *Chem. Res. Toxicol.* **2005**, *18*, 1729–1736. https://doi.org/10.1021/tx0501785.
41. Peter, D.M.; Vögeli, B.; Cortina, N.S.; et al. A Chemo-Enzymatic Road Map to the Synthesis of CoA Esters. *Molecules* **2016**, *21*, 517. https://doi.org/10.3390/molecules21040517.
42. Zhang, D.; Zhang, F.; Liu, W. A KAS-III Heterodimer in Lipstatin Biosynthesis Nondecarboxylatively Condenses C8 and C14 Fatty Acyl-CoA Substrates by a Variable Mechanism during the Establishment of a C22 Aliphatic Skeleton. *J. Am. Chem. Soc.* **2019**, *141*, 3993–4001. https://doi.org/10.1021/jacs.8b12843.
43. Nevarez, D.M.; Mengistu, Y.A.; Nawarathne, I.N.; et al. An N-Aroyltransferase of the BAHD Superfamily Has Broad Aroyl CoA Specificity *in vitro* with Analogues of N-Dearoylpaclitaxel. *J. Am. Chem. Soc.* **2009**, *131*, 5994–6002. https://doi.org/10.1021/ja900545m.
44. Pal, M.; Easton, N.M.; Yaphe, H.; et al. Potent dialkyl substrate-product analogue inhibitors and inactivators of α-methylacyl-coenzyme A racemase from Mycobacterium tuberculosis by rational design. *Bioorganic Chem.* **2018**, *77*, 640–650. https://doi.org/10.1016/j.bioorg.2018.01.041.
45. Valenzano, C.R.; You, Y.O.; Garg, A.; et al. Stereospecificity of the Dehydratase Domain of the Erythromycin Polyketide Synthase. *J. Am. Chem. Soc.* **2010**, *132*, 14697–14699. https://doi.org/10.1021/ja107344h.
46. Haslinger, K.; Brieke, C.; Uhlmann, S.; et al. The Structure of a Transient Complex of a Nonribosomal Peptide Synthetase and a Cytochrome P450 Monooxygenase. *Angew. Chem. Int. Ed.* **2014**, *53*, 8518–8522. https://doi.org/10.1002/anie.201404977.
47. Izoré, T.; Tailhades, J.; Hansen, M.H.; et al. Drosophila melanogaster nonribosomal peptide synthetase Ebony encodes an atypical condensation domain. *Proc. Natl. Acad. Sci. USA* **2019**, *116*, 2913–2918. https://doi.org/10.1073/pnas.1811194116.
48. Rosenthal, R.G.; Ebert, M.O.; Kiefer, P.; et al. Direct evidence for a covalent ene adduct intermediate in NAD(P)H-dependent enzymes. *Nat. Chem. Biol.* **2014**, *10*, 50–55. https://doi.org/10.1038/nchembio.1385.